PAPER

Check for updates

Computational study of novel 2H chromium ditelluride as an anode material for Li/K-ion batteries

Muhammad Isa Khan, [iD] *[a] Iqra Mehmood,[a] Saleh S. Alarfaji,[b] Muhammad Junaid[a] and Tahir Iqbal[c]

The goal of metal-ion battery research is to develop anode materials with high storage capacity. This study explored the potential of 2H phase $CrTe_2$, composed of two hexagonally stacked layers, as an optimal anode material for Li/K-ion batteries using Density Functional Theory (DFT). Preliminary analyses revealed that the material possesses thermodynamic, structural, and mechanical stability. A key finding was the significantly negative adsorption energy, which enhances battery stability by preventing clustering and stabilizing Li/K adsorption on the material's surface. The adsorption energy values for Li/K were calculated to be -3.7 eV and -4.63 eV, respectively. These results suggest stable lithiation and potassiation processes, with maximum storage capacities of 1395 mA h g^{-1} for Li and 1134 mA h g^{-1} for K. Additionally, the calculated open-circuit voltages (OCVs) for $CrTe_2$ were 0.13 V for K-ions and 0.20 V for Li-ions. We calculated the adsorption energy, structural and electronic properties, theoretical capacity, diffusion energy, and thermal stability. The electrical conductivity of the material increased, and its metallic properties were maintained with increasing metal-ion concentration. This study highlights the potential of $CrTe_2$ as a novel anode material for Li-/K-ion batteries.

1 Introduction

Modern hybrid vehicles and portable electronic devices have made the development of durable and efficient energy sources important. The outstanding qualities of the lithium-ion battery (LIB), including its high energy density, strong cycle performance, and lightweight design have attracted attention.[1] LIBs are essential to the transition from oil-powered to electric-powered vehicles.[2] They continue to serve as energy storage devices, aiding in the shift to renewable energy sources.[3] Furthermore, the manufacturing of lithium-ion batteries has expanded dramatically in response to the growing demand for portable electronic devices, like laptops, mobiles, tablets, digital cameras, wearable devices, and drones.[4]

The electrochemical and physical properties including the overall performance of batteries, result from the complex interaction between components such as the anode, cathode, binder, separator, and electrolyte solution. These components undergo multiple manufacturing processes that shape the structure of the battery electrodes.[5] It is crucial to fully understand how the various parts and production procedures interact and influence the unique qualities of the battery to achieve the best performance, quality, and cost-efficiency in LIB production.

Since Sony introduced LIBs in 1991, the technology has seen significant advancements. However, the growing demand has raised concerns about lithium scarcity. This has spurred efforts to explore alternatives, including sodium-ion batteries (NIBs), which have gained attention due to sodium's abundance and lower cost than lithium.[6] Going beyond NIBs, there is also ongoing research into batteries utilizing other alkali metals like multivalent metal ions, including magnesium (Mg), calcium (Ca), and aluminum (Al).

As potassium is widely affordable and environmentally friendly, potassium-ion batteries (KIBs) are emerging as a competitive alternative for large-scale electrical energy storage compared to LIBs. KIBs might be a more cost-effective and environmentally responsible option for energy storage. Researchers are actively investigating different electrode materials to understand their qualities and performance to increase their efficacy and viability for future applications. The choice of electrode material greatly impacts the stability, conductivity, cost, weight, and environmental impact of batteries. The key challenge in developing these diverse secondary batteries lies in the search for suitable electrode materials that can be tailored to optimize battery performance. This quest for electrode materials is crucial to enable them to reach their greatest

[a]Department of Physics, The Islamia University of Bahawalpur, Rahim Yar Khan Campus, Bahawalpur, Pakistan. E-mail: muhammad.isa@iub.edu.pk; iqraamehmoodch30@gmail.com; m.junaid@iub.edu.pk

[b]Department of Chemistry, Faculty of Science, King Khalid University, P. O. Box 9004, Abha 61413, Saudia Arabia. E-mail: ssalarvagi@kku.edu.sa

[c]Department of Physics, University of Gujrat, Gujrat, Pakistan

potential alternative battery technologies and address the limitations of traditional LIBs. Owing to its high particular capacity and the layered structure of electrode materials, which usually exhibit an inverse relationship with their mass density, graphite is frequently chosen as the primary electrode material. The specific capacity of these battery materials can also be enhanced due to lightweight carbon compositions.

The field of two-dimensional (2D) materials has recently seen significant research activity as a promising new class of anode materials. Their unique structure and diverse applications pique our curiosity.[7–9] Consider the 2D material pioneer graphene, which has a remarkable theoretical Li-ion storage capacity (784 mA h g^{-1})[10] a significant surface-to-mass ratio (2965 m^2 g^{-1}),[11] increased thermal conductivity,[12] and remarkable mechanical strength.[13] Its extraordinary characteristics distinguish it from its bulk form. Besides graphene, other 2D materials like bismuthene, borophene, and their interfaces have already been extensively studied for use in lithium and non-lithium ion batteries. Various 2D materials have been extensively investigated for their application in alkali metal ion, magnesium, and zinc ion batteries, demonstrating promising characteristics such as high capacity, optimal OCV, favorable thermodynamic properties, and significant adsorption energy. These attributes highlight the potential of 2D materials as effective components in advancing battery technology.[14–18]

Chalcogenides and dichalcogenides are a promising class of novel electrode materials that can be used in batteries and supercapacitors.[19,20] Compounds containing one or more chalcogen anions, such as tellurium, oxygen, selenium, and sulfur are known as dichalcogenides. Various binary and ternary chalcogenide compositions are reported in the literature.[21] Transition metal dichalcogenides (TMDs), including chromium ditelluride, are known for their semiconducting properties. The monolayer form of CrTe$_2$ exhibits a hexagonal lattice structure and possesses intriguing electrical and optical characteristics. Its adjustable band gap is a crucial characteristic that qualifies it for use in electronic devices. Furthermore, the monolayer of chromium ditelluride exhibits strong mechanical flexibility, thermal stability, and electrical conductivity. Due to its unique properties, the chromium ditelluride monolayer has the potential to enhance battery performance. We have previously investigated magnesium diboride (MgB$_2$) and tungsten ditelluride (WTe$_2$) for their applications in batteries and the detection of volatile organic compounds (VOCs). Our findings indicate that these materials possess significant potential for exploration in various fields, including gas sensing, spintronics, battery technology, and hydrogen storage applications.[22–24]

These attributes of the 2H phase CrTe$_2$ have prompted us to investigate its suitability for metal ion batteries. We concentrated on investigating the possible electrochemical characteristics of the 2H phase CrTe$_2$ monolayer. Adsorption of Li/K changes the semiconducting behavior of the CrTe$_2$ to metallic. Different characteristics such as adsorption energy, binding energy, charge analysis, density of states (DOS), band structures, OCV, storage capacity, and diffusion barrier were explored. The results showed that CrTe$_2$ is a hopeful anode material for Li/K ion batteries. Our research concludes that

CrTe$_2$ monolayers outperform other studied anode materials for Li/K-ion batteries. Their high ion storage capacities and stable metallic characteristics position them as superior candidates for advancing battery technology.

2 Computational detail

The Amsterdam Density Functional (ADF) package's DFTB and BAND components were adopted using the Slater-type Orbital (STO) approach for all of the calculations.[25] The Generalized Gradient Approximation (GGA) in conjunction with the Perdew–Burke–Ernzerhof (PBE) technique was utilized to determine the electrons' exchange of correlation interaction.[26] To depict the atomic and electronic wave functions, a thorough basis set utilizing the double zeta double polarization was used.[27] The convergence criteria for energy (10^{-5} eV), gradient- and step-convergence was set to, 0.02 eV Å and 10^{-3} Å for all structures relaxation. The structures underwent full relaxation and Self-Consistent Field (SCF) cycles.[28]

The following formula was used to calculate the adsorption energy of the Li/K atoms on CrTe$_2$.[29]

$$E_{ad} = \frac{E_{CrTe_2(Li/K)_n} - E_{CrTe_2} - nE_{Li/K}}{n} \tag{1}$$

where n is the number of Li/K atoms being adsorbed, $E_{Li/K}$ is the energy of a single Li/K atom in bulk lattice, and $E_{CrTe_2(Li/K)_n}$ and E_{CrTe_2} are the overall energies of the structure with and without Li/K. Using the formula in eqn (2), the value of OCV was computed to assess the material's performance as anode.[30]

$$OCV = \frac{E_{CrTe_2} - xE_M - E_{CrTe_2M}}{xye} \tag{2}$$

where E_{CrTe_2} and E_{CrTe_2M} represent the total energies of chromium ditelluride in pure and with Li/K adsorption. E_M is the cohesive energy of the metal Li/K. whereas, y is the electronic charge ($y = 1$) of the Li/K ion in the electrolyte.

The following formula can be used to determine the maximum theoretical capacity (CM).[31]

$$CM = \frac{x \times Z \times F}{M_{CrTe_2}} \tag{3}$$

where Z is the valency of fully ionized Li/K and x is the maximal concentration of metal ions. The molecular mass of Li/K ions adsorbed onto the CrTe$_2$ supercell is represented by M_{CrTe_2}, and F denotes Faraday's constant (26.801 mA h mol^{-1}).

3 Results and discussion

3.1 Structural and electronic properties of CrTe$_2$

Fig. 1(a–c) presents three different views of the optimized unit cell structures of the 2H phase CrTe$_2$. The unit cell of CrTe$_2$ contains one atom of Cr and 2 atoms of Te. Next, we created and optimized the 5 × 5 × 1 supercell of CrTe$_2$. We optimized the 2H phase of the CrTe$_2$ monolayer with the $P3m1$ (156) space group presented in Fig. 1(d). In the 2H structure, two layers stack on top of each other, forming a hexagonal lattice. The atoms in each layer are arranged in a hexagonal configuration,
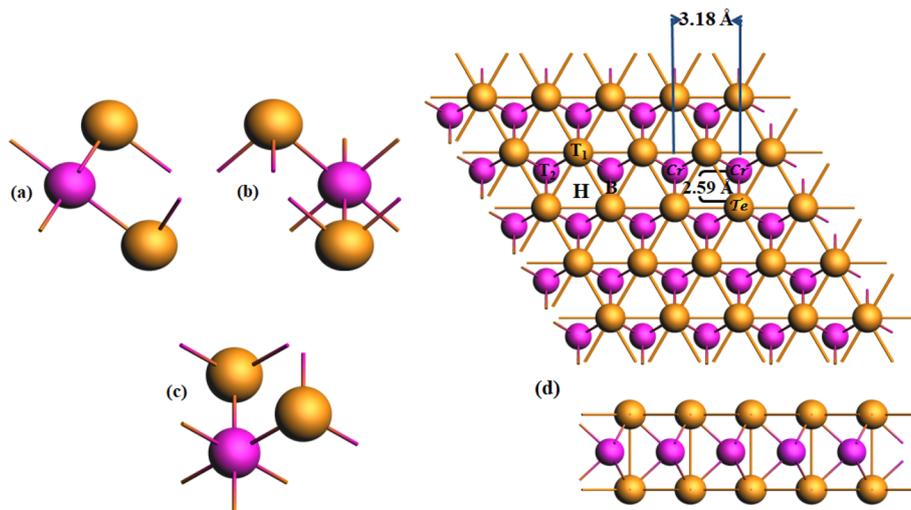
Fig. 1 The unit cell of $CrTe_2$ with different views (a) x (b) y (c) z and (d) optimized structure of $CrTe_2$ top and side view. Cr is denoted with pink and Te with golden.

and the stacking sequence repeats every two layers. Here two layers of Te atoms encircle a single layer of Cr atoms. The lattice parameter ($a = b = 3.215$ Å) values of MoS_2 are lower than the lattice parameter values ($a = b = 3.488$ Å) of $CrTe_2$.[32] However, these are smaller than those found in the monolayers of 1T-$CrTe_2$ ($a = b = 3.790$ Å) and $MoTe_2$ ($a = b = 3.550$ Å). The ideal structural bond lengths for Cr–Te, Cr–Cr, and Te–Te are approximately 2.59 Å, 3.18 Å, and 3.18 Å, respectively.

Hirshfeld charge analysis revealed a notable charge transfer from Cr ($1.275e$) to Te atoms in the 2H-$CrTe_2$, increasing electrons around the Te atoms. This occurs because the Cr atom has a lower electronegativity than the Te atom.

Chromium, with its electronic configuration of [Cr] $4s^1 3d^5$, typically forms multiple bonds influenced by its oxidation states, which range from +2 to +6, and the ligands involved. In situations where it forms more than six bonds, this involves hybridizations such as dsp^2 or d^2sp^3, utilizing its 3d, 4s, and 4p orbitals. Similarly, the electronic configuration of Te ($1s^2 2s^2 2p^6$ $3s^2 3p^6 4s^2 4p^6 4d^{10} 3d^5 5s^2$) suggests its capability to form two covalent bonds due to sp hybridization. We have applied spin-polarized calculations and found the non-magnetic nature of the $CrTe_2$. Our findings demonstrate that chromium ditelluride acts as the semiconductor with an indirect band gap of approximately 0.44 eV aligning with recent research. Bai *et al.* reported band gaps of approximately 0.52 eV using the PBE method, 0.49 eV with the PBE + SOC method, and 0.93 eV using the HSE06 functional. As mentioned in our computational details, we employed the PBE method in our calculations, so our band gap is nearly the same as the values calculated using the PBE and PBE + SOC functional.[33] Fig. 2(a) shows the DOS and (b) band structure of the pure $CrTe_2$. Analysis of the DOS reveals that the 3d orbitals of the Cr atom significantly contribute to both the valence and conduction bands, while the 4s state contributes to the valence band. The band structure results are consistent with the DOS findings.
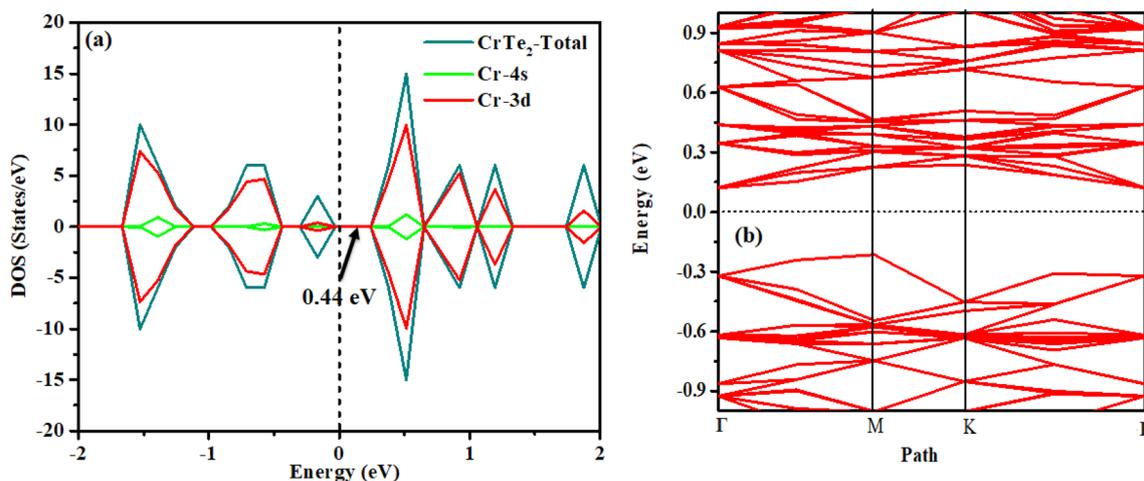

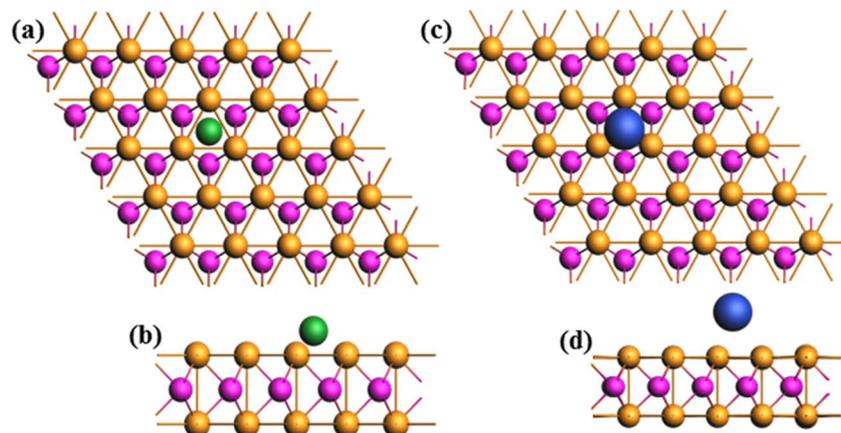**Fig. 2** Calculated (a)TDOS (b) band structure of $CrTe_2$.

Fig. 3 Optimized structure views of Li-adsorbed $CrTe_2$ (a) z, (b) x, (c) Z-view of K adsorbed $CrTe_2$ and (d) x. The Li atom is depicted in green while K is in blue.

3.2 Electronic, and adsorption properties of single Li/K atom adsorbed $CrTe_2$

The process of adsorption and removal of Li/K can lead to structural deformation, which aids in understanding its suitability as an anode material. The materials having high adsorption energy values are favorable for anode materials. This suggests that the materials with the highest adsorption energy are famous as excellent candidates for anode applications. The optimized structure of $CrTe_2$ after the adsorption of one Li/K atom is shown in Fig. 3. The adsorption of Li/K onto the 2H-$CrTe_2$ monolayer is contingent upon the charge transfers and structural environment between them to identify the most constant adsorption site. Fig. 1(d) illustrates four highly symmetric adsorption sites of $CrTe_2$ namely (i) hollow (H site) (ii) Li/K atom adsorbed at the top of Te atom (T_1 site), (iii) Cr atom (T_2 site), (iv) between the bond of Te- and Cr (B site).

A greater negative energy value indicates a more favorable location for potassium/lithium adsorption due to a stronger host contact. Table 1 shows the Li/K adsorption energy, height of the Li/K from the host material, and Hirshfeld charges at various sites. In the analysis of stable adsorption energy sites, the H site emerges as the most stable, exhibiting the lowest (most negative) adsorption energy values for both Li and K. The Li/K adsorbed $CrTe_2$ comes with adsorption energies of -3.7 eV/ -4.63 eV. For adsorption site H, the heights of lithium and

potassium are 0.02 Å, and 0.07 Å respectively. At the hexagonal ring site with the Cr atom (T_2 site), the heights of lithium and potassium are 0.15 Å, and 0.18 Å respectively. At the T_1 site on top of Te, the adsorption energy values for K and Li interactions are -3.75 eV and -4.62 eV, respectively, with corresponding heights of 0.19 Å for lithium and 0.1 Å for potassium.

Masood *et al.* employed first-principles calculations to explore the potential of WB_4 as an anode material for rechargeable alkali-metal-ion batteries. Their results indicate that Li, Na, and K adsorption on the WB_4 surface leads to remarkably high conductivity. The WB_4 monolayer efficiently adsorbs these ions, with notable adsorption energies of -2.516 eV, -2.356 eV, and -2.941 eV for Li, Na, and K ions, respectively. They also explored CrB_4 and MoB_4 by adsorbing Li/K as anode material. The adsorption energies for Li and K were $-1.31/-1.29$ eV and $-1.37/$ -1.31 eV for CrB_4/MoB_4, respectively.[29,34]

The $MoSe_2$ monolayer has been experimentally synthesized and evaluated through first-principles calculations for its potential as an anode material in different phases (1T, 1T′, and 1H). The 1T′-$MoSe_2$ monolayer shows excellent thermal, dynamical, and mechanical stability. With an adsorption energy of -1.254 eV, it prevents the formation of metallic Li clusters and becomes metallic under Li adsorption, ensuring efficient electron transport.[35] Zhao *et al.* found that TiB_2 monolayers exhibit excellent mechanical, dynamic, and thermal stability. The negative adsorption energies for Li, Na, and Mg atoms indicate favorable adsorption and prevent metallic dendrite or cluster formation. Notably, the adsorption energy values are -1.50, -1.38, and -1.48 eV for Li, Na, and Mg, respectively.[36]

In conclusion, $CrTe_2$ possesses a hexagonal layered structure with weak van der Waals forces between the layers, allowing Li/ K atoms to intercalate more easily due to the increased space and reduced resistance compared to denser materials. Furthermore, upon Li/K adsorption, $CrTe_2$ transitions from a semiconductor to a metallic state, which enhances its electronic mobility and conductivity. This improved electron transfer between the material and the adsorbed Li/K atoms reduces the adsorption energy, as the Li/K atoms can efficiently exchange electrons with the host material.

Table 1 Adsorption energy, Hirshfeld charge, and height of Li/K at various adsorption sites

Materials	Sites	E_d (eV)	$\Delta Q_{Li/K}$	Height (Å)
Li	H	-3.70	0.346	0.02
	T_1	-3.63	0.309	0.19
	T_2	-3.62	0.323	0.15
	B	-3.65	0.321	0.15
K	H	-4.63	0.517	0.07
	T_1	-4.59	0.515	0.11
	T_2	-4.58	0.506	0.18
	B	-4.61	0.513	0.17

Hirshfeld charge transfer analysis was used to assess the interaction between Li/K and the CrTe$_2$; the results are displayed in Table 1. The CrTe$_2$ monolayer gained electronic charge from adsorbed Li/K. When a single Li/K atom is adsorbed on different sites of CrTe$_2$, it transfers a charge to the CrTe$_2$ and behaves as an electron donor. The electron transfer from lithium and potassium to the CrTe$_2$ indicates that Li and K atoms are adsorbed onto the CrTe$_2$ material, suggesting a redox reaction occurring in the electrode material during battery operation, consistent with previous studies and findings (Table 2).

At the H site, Li/K transfers $0.346e/0.517e$ to the atoms of the six-membered CrTe ring. For the T$_2$ site, Li donates $0.323e$ while K donates $0.506e$ to the CrTe ring. At the T$_1$ site, Li/K transfers a charge of $0.309e/0.515e$, respectively. When a Li/K atom is adsorbed on the link between Cr and Te (B site), the transferred charge values are $0.321e$ and $0.513e$. The findings indicate that the strongest contact between Li and Cr is towards Cr atoms in

the monolayer, implying that the newly created Cr–Cr bond is more electronegative. By the adsorption energy findings, the H site appears to be the most stable due to Li/K's strong charge transfer value.

The absorption of a single Li/K atom transforms the semi-conducting nature of CrTe$_2$ into a conductor. Fig. 4(a and c) presents the DOS of Li/K adsorbed CrTe$_2$, while Fig. 4(b and d) shows the corresponding band structure. The DOS results in Fig. 4(a and c) are in good agreement with the band structure in Fig. 4(b and d).

Using the ELF, we assessed the structure's bonding properties as illustrated in Fig. 5. A molecule with an ELF value of less than 0.5 shows that it is ionic in nature whereas a high ELF value (>0.5) indicates primarily covalent bonding. An ELF value of 0.5 signifies a metallic bond.[39]

From Fig. 5(a) purple regions around the Te atoms in host material CrTe$_2$ initially show covalent bonding characteristics between Cr and Te with an ELF value of 0.75. Nevertheless, following Li/K adsorption red color around the Li/K atom shows that the structure has an ionic bonding nature with an ELF value of 0.25. The structural stability is enhanced by the coexistence of ionic and covalent bonds, which is beneficial for the adsorption of Li and K ions.

3.3 Effect of lithium/potassium concentration and stability

The system's average adsorption energy was determined by gradually adding Li/K atoms to the host material using eqn (4).
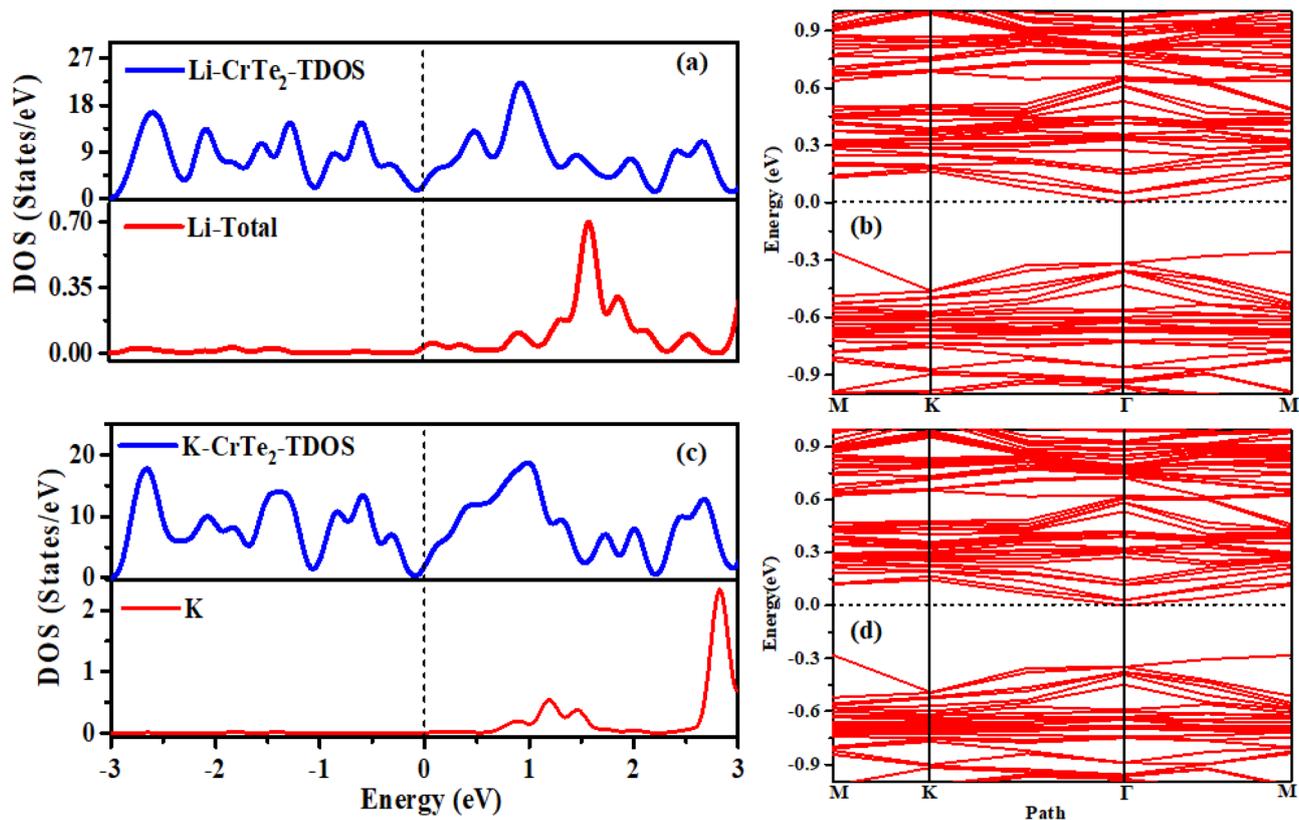
Table 2 Comparison of single Li/K adsorption energy (eV) with the literature

Material	K	Li	Ref.
CrTe$_2$	−4.63	−3.7	This work
WB$_4$	−2.94	−2.51	34
CrB$_4$	−1.37	−1.31	29
MoB$_4$	−1.31	−1.29	29
TiC$_3$	—	−0.93	37
AlB$_4$	—	2.14	38

Fig. 4 (a) DOS- (b) band structure of Li-adsorbed CrTe$_2$ (c) DOS- (d) band structure of K-adsorbed CrTe$_2$.
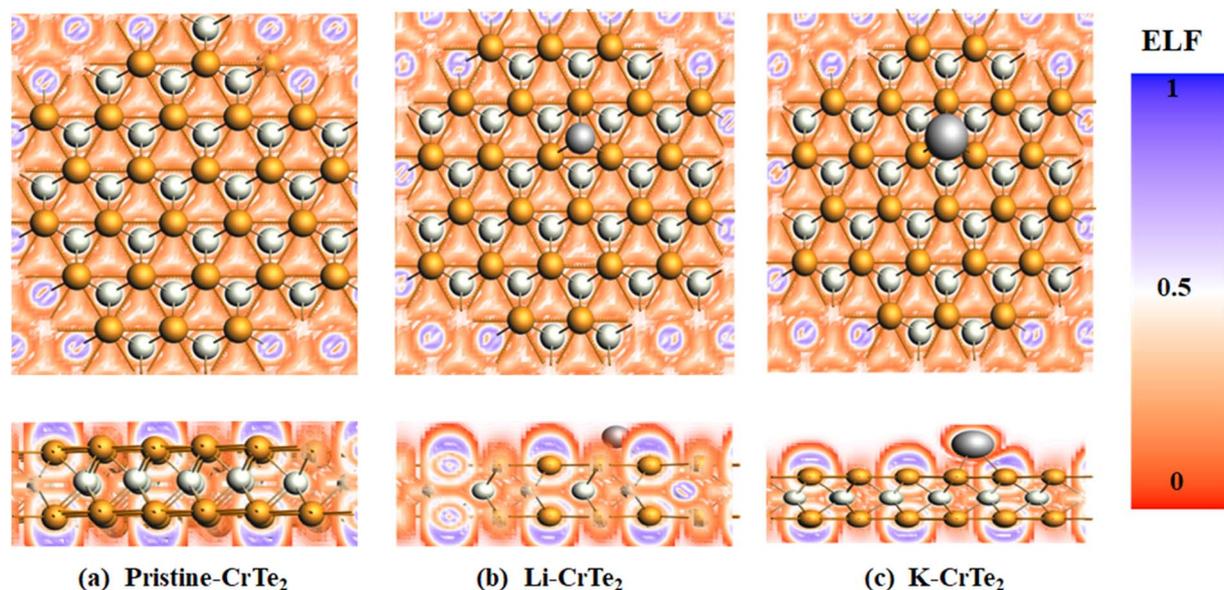
Fig. 5 The ELF maps of (a) pristine (b) Li- (c) K-adsorbed $CrTe_2$.

Fig. 6 shows the optimized structures of fully lithiated and potassiated $CrTe_2$. The concentration of Li/K atoms in $CrTe_2$ was gradually increased to calculate the adsorption energy by the following eqn (4).

$$\text{ave } E_{ads} = \frac{1}{n}(E_{MCrTe_2} - E_{CrTe_2} - nE_M) \tag{4}$$

Here, E_{MCrTe_2} is the energy of the Li/K adsorbed $CrTe_2$, while E_{CrTe_2} is the energy of the pure $CrTe_2$. E_M is the reference energy of Li/K calculated using a bulk lattice with a bcc unit cell, where n represents the number of metal atoms.

Li/K atoms were initially positioned on the top side of the $CrTe_2$ at the most favorable H site and then on the lower side. 16 Li and 13 K atoms were adsorbed one by one on the studied structure. The declining trend shown in Fig. 6(a) indicates that the lithiation/potassiation energy value approaches zero as more Li/K atoms are introduced, demonstrating the feasibility of the exothermic reaction. The potassiated structure shows positive adsorption energy when the 14th K atom is adsorbed onto $CrTe_2$, indicating that the host material will not adsorb additional atoms. The adsorption energy becomes progressively more negative upon the adsorption of 17th and 18th Li. However, with the 20th and 21st Li adsorption on $CrTe_2$, the adsorption energy starts to decrease towards zero, reaching values of −0.10 and −0.05, respectively. Therefore, we halted further calculations.
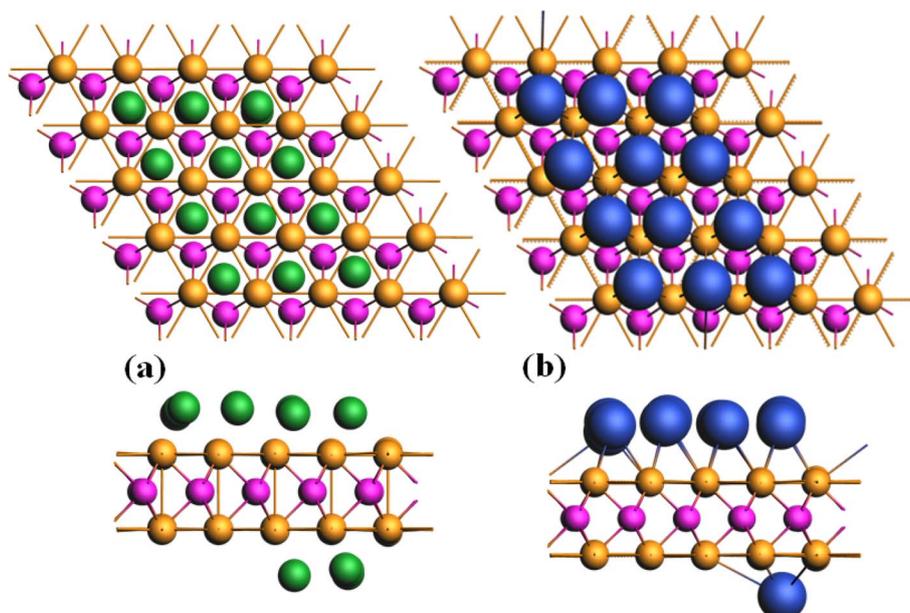

Fig. 6 The fully optimized structures (a) lithiated (b) potassiated $CrTe_2$.

The geometrical structures are found to be rather stable within the estimated adsorption energy ranges of -3.7 eV to -0.20 eV for Li and -4.63 eV to -0.13 eV for K, respectively, as the concentrations of Li and K grow. Its stability guarantees a structure free of dendrites, allowing for safe lithiation/potassiation.

Structural stability is determined by the change in the area after the adsorption of Li/K in $CrTe_2$. A structure is considered stable if it experiences minimal volume expansion after adsorption. To assess the effect of Li/K adsorption on $CrTe_2$, we calculate the change in area (ΔS) as a function of the concentration of Li/K, representing the volume expansion. This is calculated by eqn (5) given below.

$$\Delta S = \frac{\left(S_{Li/K@CrTe_2} - S_{CrTe_2} \right)}{S_{CrTe_2}} \times 100\% \qquad (5)$$

where $S_{Li/K@CrTe_2}$ represents the volume of fully lithiated/potassiated $CrTe_2$ and S_{CrTe_2} represents the volume of the pure $CrTe_2$. The adsorption of Li/K on $CrTe_2$ did not change the bond lengths of the structure. Consequently, no volume expansion occurs during the adsorption process. This stability improves the cycle capacity during the charging and discharging, making $CrTe_2$ a beneficial anode material for Li/K ion batteries.

3.4 OCV and theoretical capacity of Li/K adsorbed $CrTe_2$

The average OCV and theoretical capacity are critical attributes, as they reflect the higher capacity and energy density of metal-ion batteries in their electrochemical performance. OCV is a key feature of rechargeable ion batteries, offering insight into their functionality and storage capacity. Eqn (2) is used to compute the OCV value, and Fig. 7(b) illustrates the average OCV for Li/K at various atomic concentrations. As shown in Fig. 7(b), no negative values are observed, indicating a preference for Li/K ions to adsorb on $CrTe_2$ rather than forming metallic states. This underscores the material's suitability compared to the conventional graphite electrode.[40] The concentration of Li atoms peaks near an OCV of 3.8 V. The electrode potential voltage profile ranges between 3.8 V and 0.20 V for Li and 4.6 V to 0.13 V for K, showing a decreasing trend with increasing Li content. Low OCV range anodes for high-capacity materials are essential to ensure proper operation (Fig. 8).

Eqn (3) was used to determine the maximum capacity of $CrTe_2$ upon Li/K adsorption. The maximum capacity at the highest concentration of Li/K on $CrTe_2$ is 1395 mA h g^{-1} and 1134 mA h g^{-1}, respectively. These values exceed the useable capacity of the graphite anode, which is 372 mA h g^{-1}. Furthermore, the computed capacity for K is higher than the blue phosphorene monolayer's (570 mA h g^{-1}) capacity,[41] and Ti_3C_2 MXene (191 mA h g^{-1}).[42] On the other hand, Li has a greater estimated capacity than graphene (784 mA h g^{-1}),[42] and germanium sulphide (256 mA h g^{-1}).[43]

In this comparison, the maximum theoretical capacity for YS_2 in a lithium-ion battery is 350 mA h g^{-1} and the diffusion barrier is 0.33.[44] T Zaho et al. studied lithium-ion batteries using TiC_2. Their study results show a theoretical capacity of 622 mA h g^{-1}, a voltage of 0.94 V, and a diffusion barrier (0.11 eV).[45] C. Eamas et al. worked on lithium-ion batteries using Ti_2C, finding a theoretical capacity of 440 mA h g^{-1}, a voltage of 0.44 V, and a diffusion barrier (0.27 eV).[46] Working with Ti_2BN monolayer, Y. Y. Wu et al. discovered a theoretical capacity of 889 mA h g^{-1}, a voltage of 0.024 V, and a diffusion barrier (0.24 eV) for lithium-ion batteries.[47] H. R. Jiang et al. worked on potassium-ion batteries using BP, finding an open circuit voltage of 0.27 V and a diffusion barrier of 0.155 eV.[41] Working with 2D MON_2, X. Zong et al. discovered an open circuit voltage of 1.11 V and a diffusion barrier of 0.49 eV when studying potassium-ion batteries.[48] For potassium-ion batteries, K. Dou et al. found a voltage of 0.024 V and a diffusion barrier of 0.24 eV (Table 3).[49]
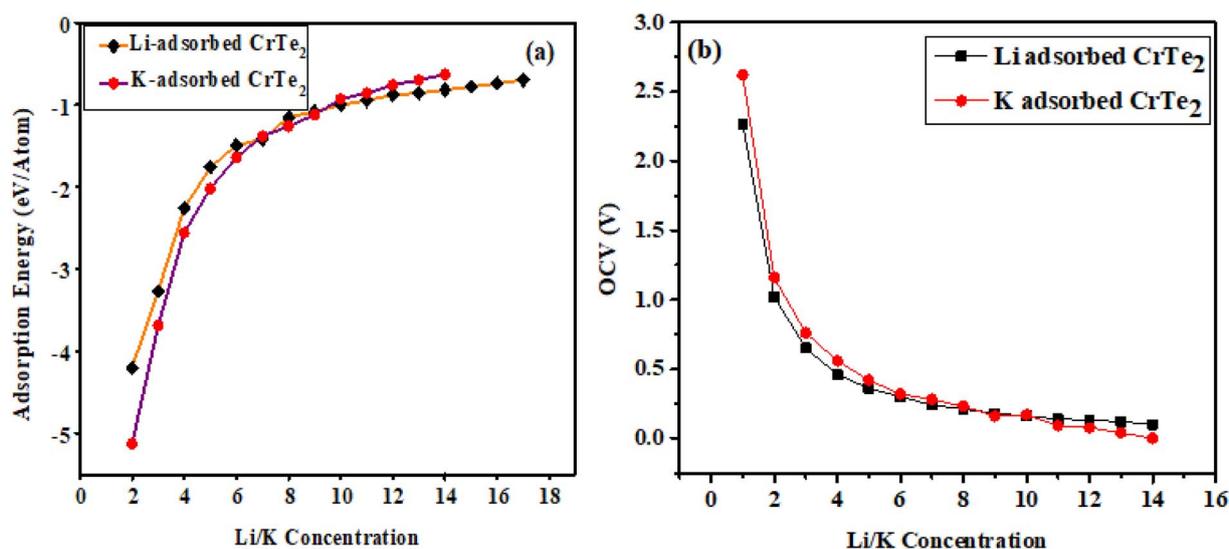

Fig. 7 (a) Average adsorption energy (b) OCV profile upon loading the Li/K on $CrTe_2$.
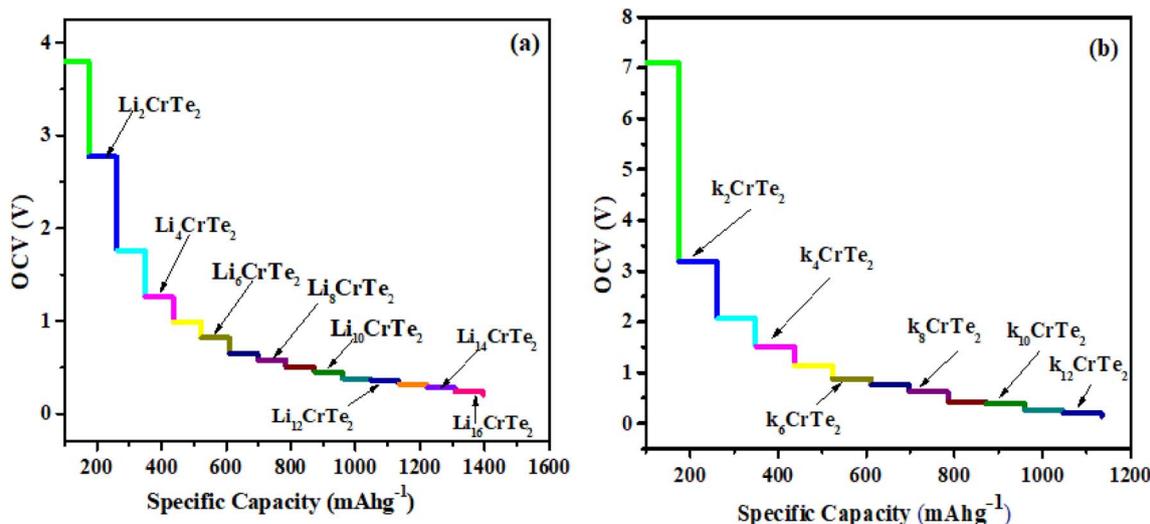
Fig. 8 Relation of OCV and specific capacity (a) Li (b) K adsorbed $CrTe_2$.

Table 3 An analysis of a few popular anode materials for LIBs/KIBs regarding diffusion barrier (eV), open circuit voltage (V), and specific theoretical capacity (mA h g^{-1})

Material	Atom	Specific capacity (mA h g^{-1})	Diffusion barrier (eV)	OCV (V)	Reference
$CrTe_2$	Li	1395	0.16	0.20	This work
YS_2	Li	350	0.33	—	44
TiC_2	Li	622	0.11	0.94	45
Ti_2C	Li	440	0.27	0.44	46
Ti_2BN	Li	889	0.24	0.024	47
$CrTe_2$	K	1134	0.26	0.13	This work
BP	K	—	0.155	0.27	41
MoN_2	K	—	0.49	1.11	48
PC	K	—	0.26	0.69	49

3.5 Diffusion analysis

Lithium diffusion plays a crucial role in the charging and discharging rates of electrode materials, making the analysis of ion mobility essential for enhancing LIB capacity. The rate capability, particularly important for high-power applications like electric vehicles, depends on the transport of lithium ions and electronic conductivity.[50,51] To address these issues, the diffusion barrier must be calculated. In this work, diffusion properties were determined using the climbing-image nudged elastic band (CI-NEB) method, which finds the highest energy point along the diffusion path.[52] The two selected diffusion pathways for Li/K are the hollow site on top of Cr/Te and the hollow site (H–Cr/Te–H). The diffusion barriers were found to be 0.26 and 0.53 eV for K, and 0.16 and 0.17 eV for Li. Therefore, $CrTe_2$ significantly enhances Li/K mobility and improves the charging/discharging capabilities when used as an anode material in Li/K ion batteries.

Regarding thermal properties, we computed the thermal energies of K and Li atoms at temperatures of 300 K and 400 K using the following relation.[53]

$$E = \frac{3}{2}K_B T \qquad (6)$$

Here K_B is the Boltzmann constant and T is the temperature in Kelvin (K). The calculated thermal energies are 6.21×10^{-2} and 8.28×10^{-21} at 300 K and 400 K respectively, which are significantly lower than their corresponding diffusion barriers. This implies that the likelihood of Li and K atoms overcoming these barriers and diffusing is negligible. Based on these diffusion barriers, $CrTe_2$–Li/K materials are energetically stable and demonstrate good rate capability, making them suitable as anodes for Li/K ion batteries.

3.6 Dynamical and thermal stability

In this research, we performed *ab initio* molecular dynamics (AIMD) simulations on a $5 \times 5 \times 1$ supercell of $CrTe_2$ at 400 K, to assess thermal stability. The key factors in determining the optimal Li/K concentration are the negative average adsorption energy and the material's thermal stability throughout the charging/discharging process. Structural changes with Li/K insertion, shown in Fig. 6, revealed no structural deformation during the fully lithiated/potassiated process, indicating structural stability.

The AIMD simulations over 10 ps at 400 K, illustrated in Fig. 9, evaluated the recovery dynamics of the $CrTe_2$ anode. The
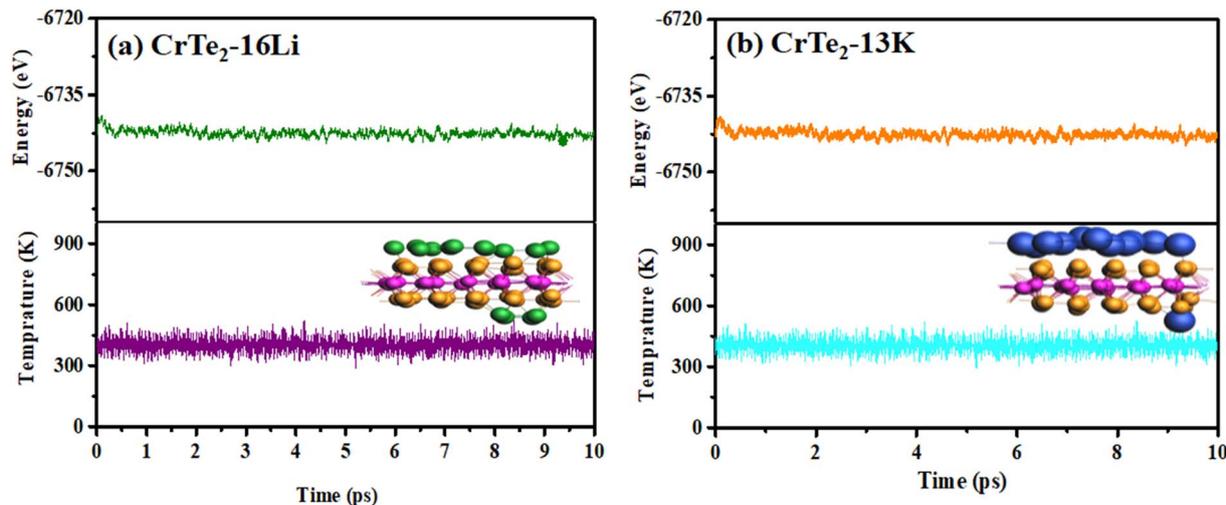
Fig. 9 The energy and temperature fluctuation *vs.* time steps (a) Li-CrTe$_2$ and (b) K-CrTe$_2$.

minimal energy variation during this MD timescale underscores the thermal stability of Li/K-adsorbed CrTe$_2$ at 400 K, as the structure remains intact with no indications of bond breaking, thereby confirming the monolayer's durability for Li/K. This suggests the stability and feasibility of the proposed material as an anode for Li/K ion batteries.

4 Conclusions

DFT calculations were employed to explore CrTe$_2$ as an anode material for Li/K ion batteries. The binding energy values for the most stable H site are −3.7 eV for Li and −4.63 eV for K. The charge transfer from Li/K to CrTe$_2$ is 0.34/0.51 eV, which is essential for anode materials to prevent clustering during the adsorption process. Li/K adsorbed CrTe$_2$ exhibits a favorable OCV of 0.20/0.13 V and a storage capacity of 1395 mA h g^{-1} for Li and 1134 mA h g^{-1} for K during the storage process. These values surpass those of the commercially available graphite anode material. In addition, 2H-CrTe$_2$ has an ultra-low diffusion barrier, indicating rapid mobility of Li/K atoms. The diffusion energy barrier is 0.16 eV for Li and 0.26 eV for K. Our proposed material demonstrated excellent cycling performance due to the absence of volume shrinkage. These results suggest that 2H-CrTe$_2$ is a promising candidate for Li/K ion batteries.

Data availability

No datasets were generated or analysed during the current study.

Conflicts of interest

The authors declare no conflict of interest.

Acknowledgements

References

1 H. Wang, L.-F. Cui, Y. Yang, H. Sanchez Casalongue, J. T. Robinson, Y. Liang, Y. Cui and H. Dai, Mn3O4−graphene hybrid as a high-capacity anode material for lithium ion batteries, *J. Am. Chem. Soc.*, 2010, **132**(40), 13978–13980.

2 A. Kwade, W. Haselrieder, R. Leithoff, A. Modlinger, F. Dietrich and K. Droeder, Current status and challenges for automotive battery production technologies, *Nat. Energy*, 2018, **3**(4), 290–300.

3 A. Manthiram, A reflection on lithium-ion battery cathode chemistry, *Nat. Commun.*, 2020, **11**(1), 1550.

4 Y. Liang, C. Z. Zhao, H. Yuan, Y. Chen, W. Zhang, J. Q. Huang, D. Yu, Y. Liu, M. M. Titirici and Y. L. Chueh, A review of rechargeable batteries for portable electronic devices, *InfoMat*, 2019, **1**(1), 6–32.

5 O. Schmidt, M. Thomitzek, F. Röder, S. Thiede, C. Herrmann and U. Krewer, Modeling the impact of manufacturing uncertainties on lithium-ion batteries, *J. Electrochem. Soc.*, 2020, **167**(6), 060501.

6 M. D. Slater, D. Kim, E. Lee and C. S. Johnson, Sodium-ion batteries, *Adv. Funct. Mater.*, 2013, **23**(8), 947–958.

7 P. G. Bruce, B. Scrosati and J. M. Tarascon, Nanomaterials for rechargeable lithium batteries, *Angew. Chem., Int. Ed.*, 2008, **47**(16), 2930–2946.

8 K. S. Novoselov, A. Mishchenko, A. Carvalho and A. Castro Neto, 2D materials and van der Waals heterostructures, *Science*, 2016, **353**(6298), aac9439.

9 D. Akinwande, C. Huyghebaert, C.-H. Wang, M. I. Serna, S. Goossens, L.-J. Li, H.-S. P. Wong and F. H. Koppens, Graphene and two-dimensional materials for silicon technology, *Nature*, 2019, **573**(7775), 507–518.

10 E. Yoo, J. Kim, E. Hosono, H.-s. Zhou, T. Kudo and I. Honma, Large reversible Li storage of graphene nanosheet families

for use in rechargeable lithium ion batteries, *Nano Lett.*, 2008, **8**(8), 2277–2282.

11 H. K. Chae, D. Y. Siberio-Pérez, J. Kim, Y. Go, M. Eddaoudi, A. J. Matzger, M. O'keeffe, O. M. Yaghi, M. Design and D. Group, A route to high surface area, porosity and inclusion of large molecules in crystals, *Nature*, 2004, **427**(6974), 523–527.

12 A. A. Balandin, S. Ghosh, W. Bao, I. Calizo, D. Teweldebrhan, F. Miao and C. N. Lau, Superior thermal conductivity of single-layer graphene, *Nano Lett.*, 2008, **8**(3), 902–907.

13 C. Lee, X. Wei, J. W. Kysar and J. Hone, Measurement of the elastic properties and intrinsic strength of monolayer graphene, *science*, 2008, **321**(5887), 385–388.

14 M. I. Khan, G. Nadeem, A. Majid and M. Shakil, A DFT study of bismuthene as anode material for alkali-metal (Li/Na/K)-ion batteries, *Mater. Sci. Eng., B*, 2021, **266**, 115061.

15 M. I. Khan, M. Khurshid, S. S. Alarfaji and A. Majid, Bismuthene for novel anode material of Magnesium/Zinc ion batteries with high capacity and stability: A DFT calculation, *Phys. Chem. Chem. Phys.*, 2024, DOI: 10.1039/D4CP03154G.

16 M. I. Khan, M. Anwar, A. Majid, M. Shakil and M. Rizwan, Computational studies of super-B as anodes for AM (Li, Na, and K) ion batteries, *J. Electrochem. Soc.*, 2022, **169**(9), 090514.

17 M. I. Khan, A. Majid, N. Ashraf and I. Ullah, A DFT study on a borophene/boron nitride interface for its application as an electrode, *Phys. Chem. Chem. Phys.*, 2020, **22**(6), 3304–3313.

18 M. I. Khan, S. Aslam, A. Majid and S. S. A. Gillani, Intercalation of Lithium inside bilayer buckled borophene: a first principles prospective, *J. Electrochem. Soc.*, 2021, **168**(7), 070535.

19 M. Sajjad, F. Cheng and W. Lu, Research progress in transition metal chalcogenide based anodes for K-ion hybrid capacitor applications: a mini-review, *RSC Adv.*, 2021, **11**(41), 25450–25460.

20 I. Ullah, A. Majid and M. I. Khan, Gadolinium-based olivine phosphate for upgradation of cathode material in lithium ion battery, *J. Mater. Sci.: Mater. Electron.*, 2020, **31**, 7324–7334.

21 S. Song, Y. Sim, S.-Y. Kim, J. H. Kim, I. Oh, W. Na, D. H. Lee, J. Wang, S. Yan and Y. Liu, Wafer-scale production of patterned transition metal ditelluride layers for two-dimensional metal–semiconductor contacts at the Schottky–Mott limit, *Nat. Electron.*, 2020, **3**(4), 207–215.

22 M. I. Khan, A. Saeed, M. Shakil, G. Saira, A. Ahmad, F. Imam and S. S. Alarfaji, Computational exploration of high-capacity hydrogen storage in alkali metal-decorated MgB2 material, *J. Power Sources*, 2024, **613**, 234881.

23 J. Hafeez, M. U. Islam, S. M. Ali, S. Khalid and N. Ashraf, Computational exploring the potential of pure and Ag-decorated WTe2 for detecting volatile organic compounds (VOCs), *Mater. Sci. Semicond. Process.*, 2024, **182**, 108710.

24 R. Gilani, S. S. Alarfaji, K. Nadeem, A. Saeed and M. I. Khan, Pristine and aurum-decorated tungsten ditellurides as sensing materials for VOCs detection in exhaled human breath: DFT analysis, *RSC Adv.*, 2024, **14**(37), 26788–26800.

25 G. T. Te Velde, F. M. Bickelhaupt, E. J. Baerends, C. Fonseca Guerra, S. J. van Gisbergen, J. G. Snijders and T. Ziegler, Chemistry with ADF, *J. Comput. Chem.*, 2001, **22**(9), 931–967.

26 J. P. Perdew, K. Burke and M. Ernzerhof, Generalized gradient approximation made simple, *Phys. Rev. Lett.*, 1996, **77**(18), 3865.

27 F. Jensen, Polarization consistent basis sets. II. Estimating the Kohn–Sham basis set limit, *J. Chem. Phys.*, 2002, **116**(17), 7372–7379.

28 P. Császár and P. Pulay, Geometry optimization by direct inversion in the iterative subspace, *J. Mol. Struct.*, 1984, **114**, 31–34.

29 M. K. Masood, J. Wang, J. Song and Y. Liu, A novel two-dimensional whorled CrB4 and MoB4 as high-performance anode material for metal ion batteries, *Appl. Surf. Sci.*, 2024, **652**, 159301.

30 X. Zhang, J. Hu, Y. Cheng, H. Y. Yang, Y. Yao and S. A. Yang, Borophene as an extremely high capacity electrode material for Li-ion and Na-ion batteries, *Nanoscale*, 2016, **8**(33), 15340–15347.

31 X. He, A. Tang, Y. Li, Y. Zhang, W. Chen and S. Huang, Theoretical studies of SiC van der Waals heterostructures as anodes of Li-ion batteries, *Appl. Surf. Sci.*, 2021, **563**, 150269.

32 C. Ataca, M. Topsakal, E. Akturk and S. Ciraci, A comparative study of lattice dynamics of three-and two-dimensional MoS2, *J. Phys. Chem. C*, 2011, **115**(33), 16354–16361.

33 S. Bai, S. Tang, M. Wu, D. Luo, J. Zhang, D. Wan and X. Li, Chromium ditelluride monolayer: A novel promising 2H phase thermoelectric material with direct bandgap and ultralow lattice thermal conductivity, *J. Alloys Compd.*, 2023, **930**, 167485.

34 M. K. Masood, K. Liu, J. Wang, J. Song and Y. Liu, Theoretical prediction of stable WB4 monolayer as a high-capacity anode material for alkali-metal ion batteries, *J. Phys. Chem. Solids*, 2024, **186**, 111814.

35 Y. Liu, X. Zhang, C. Li, N. Gao and H. Li, MoSe2 monolayer as a two-dimensional anode material for lithium-ion batteries: A first-principles study, *Colloids Surf., A*, 2024, 134455.

36 Y. Zhao, D. Chen, Y. Zheng and Y. Sun, Ab Initio Prediction and Characterization of TiB2 as a Two-Dimensional Dirac Anode for Metal (Li/Na/Mg) Ion Batteries, *Energy Fuels*, 2024, **38**(17), 17064–17075.

37 J. Park and S. A. Fatima, A DFT study of TiC3 as anode material for Li-ion batteries, *Appl. Surf. Sci.*, 2023, **638**, 158024.

38 S. Ma, H. Zhang, Z. Cheng, X. Xie, X. Zhang, G. Liu and G. Chen, Two dimensional AlB4 as high-performance anode material for Li/Na-ion batteries, *Appl. Surf. Sci.*, 2024, **648**, 159024.

39 B. Wan, Q. He, X. Wan and Q. Li, Porous hydrogen substituted graphyne as a promising anode for lithium-ion batteries, *RSC Adv.*, 2021, **11**(36), 22079–22087.

40 D. Odkhuu, D. H. Jung, H. Lee, S. S. Han, S.-H. Choi, R. S. Ruoff and N. Park, Negatively curved carbon as the anode for lithium ion batteries, *Carbon*, 2014, **66**, 39–47.

41 H. Jiang, W. Shyy, M. Liu, L. Wei, M. Wu and T. Zhao, Boron phosphide monolayer as a potential anode material for alkali metal-based batteries, *J. Mater. Chem. A*, 2017, **5**(2), 672–679.

42 D. Er, J. Li, M. Naguib, Y. Gogotsi and V. B. Shenoy, Ti3C2 MXene as a high capacity electrode material for metal (Li, Na, K, Ca) ion batteries, *ACS Appl. Mater. Interfaces*, 2014, **6**(14), 11173–11179.

43 J. Li, G. A. Tritsaris, X. Zhang, B. Shi, C. Yang, S. Liu, J. Yang, L. Xu, J. Yang and F. Pan, Monolayer honeycomb borophene: A promising anode material with a record capacity for lithium-ion and sodium-ion batteries, *J. Electrochem. Soc.*, 2020, **167**(9), 090527.

44 Y. Guo, T. Bo, Y. Wu, J. Zhang, Z. Lu, W. Li, X. Li, P. Zhang and B. Wang, YS2 monolayer as a high-efficient anode material for rechargeable Li-ion and Na-ion batteries, *Solid State Ionics*, 2020, **345**, 115187.

45 T. Zhao, S. Zhang, Y. Guo and Q. Wang, TiC 2: a new two-dimensional sheet beyond MXenes, *Nanoscale*, 2016, **8**(1), 233–242.

46 C. Eames and M. S. Islam, Ion intercalation into two-dimensional transition-metal carbides: global screening for new high-capacity battery materials, *J. Am. Chem. Soc.*, 2014, **136**(46), 16270–16276.

47 Y.-Y. Wu, T. Bo, X. Zhu, Z. Wang, J. Wu, Y. Li and B.-T. Wang, Two-dimensional tetragonal Ti2BN: A novel potential anode material for Li-ion batteries, *Appl. Surf. Sci.*, 2020, **513**, 145821.

48 X. Zhang, Z. Yu, S.-S. Wang, S. Guan, H. Y. Yang, Y. Yao and S. A. Yang, Theoretical prediction of MoN 2 monolayer as a high capacity electrode material for metal ion batteries, *J. Mater. Chem. A*, 2016, **4**(39), 15224–15231.

49 K. Dou, Y. Ma, T. Zhang, B. Huang and Y. Dai, Prediction of two-dimensional PC 6 as a promising anode material for potassium-ion batteries, *Phys. Chem. Chem. Phys.*, 2019, **21**(47), 26212–26218.

50 L. Shi, T. Zhao, A. Xu and J. Xu, Ab initio prediction of borophene as an extraordinary anode material exhibiting ultrafast directional sodium diffusion for sodium-based batteries, *Sci. Bull.*, 2016, **61**(14), 1138–1144.

51 R. H. Miwa and W. L. Scopel, Lithium incorporation at the MoS2/graphene interface: an ab initio investigation, *J. Phys.: Condens. Matter*, 2013, **25**(44), 445301.

52 G. Henkelman, B. P. Uberuaga and H. Jónsson, A climbing image nudged elastic band method for finding saddle points and minimum energy paths, *J. Chem. Phys.*, 2000, **113**(22), 9901–9904.

53 A. Kundu and B. Chakraborty, Yttrium doped covalent triazine frameworks as promising reversible hydrogen storage material: DFT investigations, *Int. J. Hydrogen Energy*, 2022, **47**(71), 30567–30579.